# POD Based Control of Beam Vibrations: Methodology and Experimental Implementation

**Gregory P. Hicks and Brian M. Lewis**
**Department of Mathematics**
**North Carolina State University**
**Center for Research in Scientific Computation**
**Box 8205 NCSU**
**Raleigh, NC 27695-8205**
**USA**

**Abstract**

The objective of this paper is to present the status of a study to determine the feasibility, through simulation, of real time implementation of control methodologies for the attenuation of beam vibrations in a smart structure paradigm caused by a narrow-band exogenous force. By narrow-band exogenous force we mean a periodic force over a narrow frequency band or a particular harmonic. The particular control methods are based on the minimization of two specific quadratic cost functionals. One of these cost functionals is a typical cost functional constrained by an affine plant. The other is a cost functional that is frequency dependent. These control methods have been used successfully in various applications; however, this investigation differs from other works in that it emphasizes the development of control methodologies based on reduced order models derived from physical first principles. In particular a central part of this focus is the Proper Orthogonal Decomposition (POD) reduction technique and its application to real-time control of beam vibrations. Numerical results indicate that POD based control achieves comparable control attenuation with full order model based control.

# 1 Introduction

Piezoceramics, usually referred to as PZT materials or PZTs, are being used in various applications including acoustics, structures, and medicine. PZT materials exhibit electromechanical properties which can be utilized in actuator and/or sensor design. In particular, they enhance their physical dimensions when an electric voltage is applied to the material while a mechanical change in the dimension of the material induces a voltage difference across the material. This actuator/sensor duality classifies PZTs as smart materials. A structure that makes use of these smart materials are known as smart structures. This investigation addresses, from a broad perspective, the feasibility of implementation of control methodologies for smart structures that make use of PZTs. In many situations, the object of PZT is to use its actuation capability to remove or minimize vibrations of the structure to which or in which it is molded or embedded.

In this paper, we are concerned with an aluminum beam to which two PZT patches are mounted in a symmetric fashion to the front and back thereof. The sensing device assumed for observation is a proximity probe and thus the effects on the beam (an extremely thin metallic surface surmounted on the beam) are assumed to be negligible and are not taken into account in the modelling of the beam. Also, it is assumed that the the beam vibration occurs transversely, a reasonable assumption for beams that have relatively small thickness when compared to width, and hence we can make use of the Euler-Bernoulli beam model. We chose to demonstrate the ideas in the context of a thin beam but the extension of analogous control techniques for more complex systems is rather straight forward.

We have focused a study on real time implementation of controls for the cantilever beam that are effective on known exogenous forces. In particular, persistent sinusoidal vibrational disturbance is introduced via the front patch of this beam and we attempt to attenuate this disturbance . The control methodologies reported on herein are two quadratic cost functional based controllers for a linear affine plant. One of these controllers is a so-called frequency shaping controller. There is a great interest in such controllers in this particular context as they are seemingly designed to deal more effectively with vibrational displacement. The use of frequency shaping on a cantilever beam with one piezoceramic patch and a uniform periodic exogenous force was previously explored in [12]. However, the difference in this study and that of [12] is two-fold. First, we have used the patch for local vibrational disturbance, as this is something that can actually be carried out experimentally in the Center for Research and Scientific Computation (CRSC) laboratory, where a beam has been constructed for experimentation (we will refer to this beam throughout as the "CSRC beam"). This is opposed to uniform forcing as discussed in [12]. Secondly, we are planning on implementing the studied controls in real-time. Accordingly, in simulation we implement the system in a discretized fashion and invoke the use of an observer instead of assuming full state feedback. Additionally, we have taken into consideration the dimension of the system. The dimension and thus computational and numerical problems of the observer based controllers are reduced by implementing a reduced order observer based on Proper Orthogonal Decomposition (POD).

The POD basis reduction method is becoming quite prolific amongst control practitioners for decreasing the complexity and dimension of systems. The popularity of POD can be attributed to the method's ability to accurately represent system data with a small number of basis elements. The POD method extracts characteristic system information from the data set via an orthogonalization process. The system data can be attained via experiment or simulation of a system and thus also lends itself well to preparatory studies like such as this one. POD has been used successfully in a variety of applications including turbulent coherent flows [3, 6, 7, 9, 14, 22], structures [17, 18, 19, 20, 21], and materials processing [10, 11, 15, 16, 24]. Furthermore, POD is found to be useful in the setting of feedback control, as found in [1, 2, 10, 11, 13]. In particular, the POD method has some history with the beam model that we are using and the CRSC beam. In [23], a POD reduced order observer was used to effectively control a transverse beam vibration due to transient pulsation utilizing

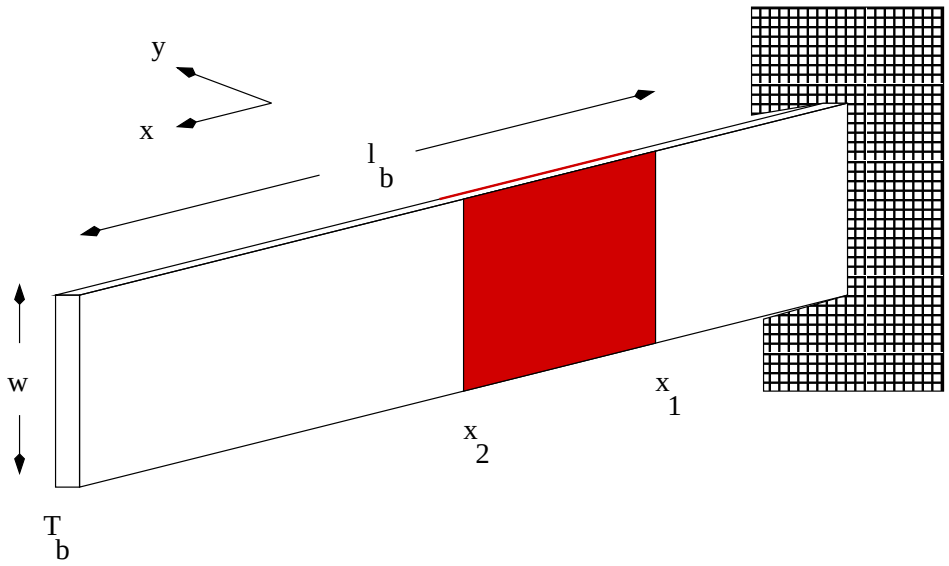


Figure 1: Cantilever beam with Piezoelectric Patches.

LQR methodology. Our study is analogous that of [23].

The organization of this paper is as follows. In Section 2, we summarize the Euler-Bernoulli beam model derivation, its solvability, and solution approximation. The POD method for reducing the order of the resulting finite-dimensional system is discussed in section 3. A brief description of the control methodologies is given in section 4. Lastly, in section 5 we describe the real time implementation simulation procedure and general discussions are provided in section 6.

# 2 The Beam Model

In this section the description of the beam model and the approximation utilized to solve it is presented. To this end consider a flat rectangular cantilevered beam, satisfying the Euler-Bernoulli displacement and Kelvin-Voigt damping hypotheses, to which piezoelectric patch actuators are mounted in a symmetric and opposing manner. The beam and patch dimensions of length $l$, width $w$, and thickness $T$, will be marked by respective subscripts $b$ and $p$ to clarify to which object's dimensions we refer, the beam or the patch. Likewise, the beam and patch material properties, Young's modulus $E$, internal damping $c_D$, and volumetric mass density $\rho$, are labelled similarly. Impose a coordinate system with $x$-direction along the length of the beam and $y$-direction along the direction of transverse displacement. Take the end located at $x = 0$ to be the clamped end of this beam. Consequently, the end located at $x = l_b$ is free. The patch edges along the beam length are denoted by $x_1$ and $x_2$. It is also assumed that the width of the beam and of the patches is the same. Thus we refer to both quantities simply by $w$. This beam is illustrated in Figure 1.

The transverse displacements $y(t, x)$ of the beam, subjected only to forces and moments

due to the patches and viscous air damping, are given by

$$\rho(x)\frac{\partial^2 y}{\partial t^2} + \gamma\frac{\partial y}{\partial t} + \frac{\partial^2 (M_x)}{\partial x^2} + \frac{\partial^2 (M_x)_p}{\partial x^2} = 0 \ , \tag{2.1}$$

where

$$\begin{gathered}\rho(x) = \rho_b T_b w + 2\rho_p T_p w \chi_{[x_1,x_2]}(x) \ , \\ (M_x)_p(t,x) = -\mathcal{K}\chi_{[x_1,x_2]}(x)[V_1(t) - V_2(t)] \ , \quad \mathcal{K} = -\tfrac{1}{2}E_p w d_{31}(T_b + T_p) \ , \end{gathered} \tag{2.2}$$

$$M_x(t,x) = EI(x)\frac{\partial^2 y}{\partial x^2}(t,x) + c_D I(x)\frac{\partial^3 y}{\partial x^2 \partial t}(t,x) \ , \tag{2.3}$$

$$EI(x) = E_b\tfrac{T_b^3 w}{12} + \tfrac{2w}{3}E_p a_3 \chi_{[x_1,x_2]}(x) \ , \quad c_D I(x) = c_{Db}\tfrac{T_b^3 w}{12} + \tfrac{2w}{3}c_{Dp} a_3 \chi_{[x_1,x_2]}(x) \ ,$$

and

$$a_3 = (T_b/2 + T_p)^3 - T_b^3/8 \ .$$

Here, $\gamma$ and $d_{31}$ are, respectively, air damping and piezoelectric strain parameters, $\chi$ indicates the characteristic function, and $V_1$ and $V_2$, respectively, represent the voltages applied to the front and back piezoelectric patches. Coupled with this partial differential equation are the boundary and initial conditions

$$y(t,0) = \frac{\partial y}{\partial x}(t,0) = 0 \ , \qquad M_x(t,\ell) = \frac{\partial}{\partial x}M_x(t,\ell) = 0 \ , \tag{2.4}$$

$$y(0,x) = y_0(x) \ , \qquad \frac{\partial y}{\partial t}(0,x) = y_1(x) \ . \tag{2.5}$$

For derivation of the beam model we refer the interested reader to [5].

Letting $\dot{y} = \frac{\partial y}{\partial t}$ and $y' = \frac{\partial y}{\partial x}$ and dropping dependence notation, equations (2.1) and (2.3) are rewritten as

$$\rho\ddot{y} + \gamma\dot{y} + M_x'' + (M_x)_p'' = 0 \ , \tag{2.6}$$

and

$$M_x = EIy'' + c_D I\dot{y}'' \ . \tag{2.7}$$

By requiring the necessary smoothness of $y$ and $\dot{y}$, namely that they are in $V = H_L^2(0,l_b) = \{\varphi \in H^2(0,l_b) \mid \varphi(0) = \varphi'(0) = 0\}$, and utilizing the boundary conditions and integration by parts one arrives at

$$\begin{gathered}\langle\rho\ddot{y},\varphi\rangle + \langle EIy'',\varphi''\rangle + \langle c_D I\dot{y}'',\varphi''\rangle + \langle\gamma\dot{y},\varphi\rangle \\ = \left\langle\mathcal{K}\chi_{[x_1,x_2]}[V_1 - V_2],\varphi''\right\rangle \ ,\end{gathered} \tag{2.8}$$

$\forall\varphi \in V$, from equation (2.6) upon substitution of equation (2.7). Equation (2.8) is written in terms of the usual inner product of $H = L^2(0,l_b)$. We now seek a function $y$, with $(y,\dot{y}) \in V \times V$, that satisfies (2.8) $\forall\varphi \in V$, a.e. $t \in (0,T_f)$ ($T_f$ some appropriately chosen final time), and (2.5).

Consider $H$ endowed with the equivalent inner product defined by $\langle v_1, v_2\rangle_H = \langle\rho v_1, v_2\rangle$ for $v_1, v_2 \in V$ . Then $V \hookrightarrow H \cong H^* \hookrightarrow V^*$, thus forming a Gelfand triple with pivot space $H$.

This triple is endowed with a duality pairing $\langle \cdot, \cdot \rangle_{V^*,V}$ defined by extending $\langle \cdot, \cdot \rangle_H$ on $V \times H$ to $V^* \times H$ via continuity. Defining

$$\sigma_1(v_1, v_2) = \langle EIv_1'', v_2'' \rangle \ , \quad \sigma_2(v_1, v_2) = \langle c_D I v_1'', v_2'' \rangle + \langle \gamma v_1, v_2 \rangle \ ,$$

and

$$\begin{aligned} q(t) &= \mathcal{K}\chi_{[x_1,x_2]}[V_1 - V_2] \\ &= \mathcal{K}\chi_{[x_1,x_2]}V_1 - \mathcal{K}\chi_{[x_1,x_2]}V_2 \\ &= f(t) + b(t) \ , \end{aligned}$$

where

$$f(t) = \mathcal{K}\chi_{[x_1,x_2]}V_1 \ , \quad b(t) = -\mathcal{K}\chi_{[x_1,x_2]}V_2 \ ,$$

(2.8) is rewritten as

$$\begin{aligned} &\langle \ddot{y}(t), \varphi \rangle_{V^*,V} + \sigma_2(\dot{y}(t), \varphi) + \sigma_1(y(t), \varphi) = \langle q(t), \varphi \rangle_{V^*,V} \ , \\ &\quad y(0,x) = y_0(x) \ , \quad \tfrac{\partial y}{\partial t}(0,x) = y_1(x) \ . \end{aligned} \tag{2.9}$$

$\forall \varphi \in V$, a.e. $t \in (0, T_f)$. From [4], under the assumption that $y_0 \in V$, $y_1 \in H$, and $q \in L^2((0,T_f); V^*)$, there exists a unique solution $y \in L^2(0,T_f;V)$ to equation (2.9) with $\dot{y} \in L^2(0,T_f;V)$ and $\ddot{y} \in L^2(0,T_f;V^*)$. This solution depends continuously on the data $(y_0, y_1, q)$.

We now describe the Galerkin approximation of the solution $y$ to (2.9). For positive integer $n$, impose an extended uniform mesh along the beam length defined by $\{x_i\}_{i=-3}^{n+3}$, where $x_i = ih$, $h = \frac{l_b}{n}$. On this mesh define the spline basis $\{s_j\}_{j=-1}^{n+1}$ by

$$s_j(x) = \frac{1}{h^3} \begin{cases} (x_{j+2} - x)^3, & x_{j+1} \le x \le x_{j+2} \\ -3(x_{j+1} - x)^3 + 3h(x_{j+1} - x)^2 + 3h^2(x_{j+1} - x)^3 + h^3, & x_j \le x \le x_{j+1} \\ -3(x - x_{j-1})^3 + 3h(x - x_{j-1})^2 + 3h^2(x - x_{j-1})^3 + h^3, & x_{j-1} \le x \le x_j \\ (x - x_{j-2})^3, & x_{j-2} \le x \le x_{j-1} \\ 0 \ , & \text{otherwise.} \end{cases}$$

From this spline basis a basis that conforms to the boundary conditions at the clamped end, $x = 0$, is formed. This basis is $\mathcal{B}^n = \{\varphi_j\}_{j=1}^{n+1}$ and is defined by

$$\varphi_j(x) = \begin{cases} -2s_{-1}(x) + s_0(x) - 2s_1(x) \ , & j = 1 \\ s_j(x) \ , & 2 \le j \le n+1. \end{cases}$$

It is clear that $span\{\mathcal{B}^n\} \subset V$.

From the spaces $span\{\mathcal{B}^n\}$ we define a semi-discrete Galerkin approximation to the solution $y$ of (2.9). Consider (2.9) restricted to $span\{\mathcal{B}^n\}$, which is

$$\begin{aligned} &\langle \ddot{y}^n(t), \varphi \rangle_H + \sigma_2(\dot{y}^n(t), \varphi) + \sigma_1(y^n(t), \varphi) = \langle q(t), \varphi \rangle_{V^*,V} \ , \\ &\quad y_0^n = y^n(0) = P^n y_0 \ , \quad y_1^n = \dot{y}^n(0) = P^n y_1 \ , \end{aligned} \tag{2.10}$$

$\forall \varphi \in span\{\mathcal{B}^n\}$, where $P^n$ is the projection of $V$ onto $span\{\mathcal{B}^n\}$. Due to the finite dimensional nature of this equation a solution is easily obtained. Selecting a solution candidate with the form $y^n(t) = \sum_{i=1}^{n+1} \eta_{in}(t)\varphi_i$, $\varphi_i \in \mathcal{B}^n$, it is noted that due to finite dimensionality and linearity one need only determine the $\eta_{in}(t)$ such that (2.10) holds for each $\varphi_j \in \mathcal{B}^n$. To find these $\eta$ first note that $\dot{y}^n(t) = \sum_{i=1}^{n+1} \dot{\eta}_{in}(t)\varphi_i$ and $\ddot{y}^n(t) = \sum_{i=1}^{n+1} \ddot{\eta}_{in}(t)\varphi_i$. Hence, upon substitutions of these expressions into equation (2.10) and the use of linearity of each of the forms and products one arrives at the expression

$$\sum_{i=1}^{n+1} \ddot{\eta}_{in} \langle \varphi_i, \varphi_j \rangle_H + \sum_{i=1}^{n+1} \dot{\eta}_{in} \sigma_2(\varphi_i, \varphi_j) + \sum_{i=1}^{n+1} \eta_{in} \sigma_1(\varphi_i, \varphi_j) = \langle q(t), \varphi_j \rangle_{V^*,V} \ ,$$

for $j = 1, \ldots, (n+1)$. Let $m_{ji} = \langle \varphi_i, \varphi_j \rangle_H$, $k_{ji} = \sigma_2(\varphi_i, \varphi_j)$, $d_{ji} = \sigma_1(\varphi_i, \varphi_j)$, $F_j(t) = \langle f(t), \varphi_j \rangle$, and $B_j(t) = \langle b(t), \varphi_j \rangle$; $j = 1, \ldots, n+1$. Furthermore, let $\beta = [\eta_{1n}, \ldots, \eta_{(n+1)n}]^T$, $M = [m_{ji}]$, $K = [k_{ji}]$, $D = [d_{ji}]$, $\vec{F}(t) = [F_1(t), \ldots, F_{n+1}(t)]^T$, and $\vec{B}(t) = [B_1(t), \ldots, B_{n+1}(t)]^T$. Under these definitions the system is rewritten as

$$M\ddot{\beta}(t) + K\dot{\beta}(t) + D\beta(t) = \vec{F}(t) + \vec{B}(t) \ . \tag{2.11}$$

Now, since $y_0^n$ and $y_1^n$ are elements of $span\{\mathcal{B}^n\}$, they have real vector representations with respect to the $\varphi_i$, say $\beta_0$ and $\beta_1$, respectively. It is easily shown that $\vec{F} + \vec{B}$ is integrable, which implies this finite dimensional system has a unique solution on $(0, T_f)$. This means that the $\eta$'s are uniquely determined and that they have all necessary regularity to ensure that the proposed solution $y^n(t)$ to (2.10) is correct. So, define the Galerkin approximation sequence $\{y^n\}_{n=1}^{\infty}$. As discussed in [5], it can be shown that $y^n \to y$, where $y$ is the unique solution to (2.9). Hence, $y^n$ is used, for sufficiently large $n$, as a model for the transverse vibrations of the beam described herein. We take $n = 16$. For the sake of implementation, we rewrite (2.11) in first order form as

$$\dot{w}(t) = Aw(t) + Bu(t) + Fg(t) \ , \tag{2.12}$$

where

$$A = \begin{bmatrix} 0 & I \\ -M^{-1}D & -M^{-1}K \end{bmatrix},$$

$$Bu(t) = \begin{bmatrix} 0 \\ M^{-1}\vec{B}(t) \end{bmatrix}, \ Fg(t) = \begin{bmatrix} 0 \\ M^{-1}\vec{F}(t) \end{bmatrix},$$

with $w_0 = [\beta_0, \beta_1]^T$. Here, $g$ and $u$ are simply new names for $V_1$ and $V_2$, respectively. Accompanying this ODE is the linear displacement observation relation

$$w_{ob} = C(\hat{x})w = Cw \ ,$$

where

$$C(\hat{x}) = \begin{bmatrix} \varphi_1(\hat{x}) & \ldots & \varphi_{n+1}(\hat{x}) & 0^{1\times(n+1)} \end{bmatrix} \ ,$$

| Beam | Patch |
|---|---|
| $\ell_b = 0.286\ m$ | $T_p = 5.3 \times 10^{-4}\ m$ |
| $T_b = 0.001\ m$ | $\rho_p = 6.599624200939254 \times 10^3\ kg/m^3$ |
| $w = 0.02543\ m$ | $E_p = 5.669533051596290 \times 10^{10}\ N/m^2$ |
| $\rho_b = 2.779661149692118 \times 10^3\ kg/m^3$ | $c_{Dp} = 5.394028447910560 \times 10^5\ Ns/m^2$ |
| $E_b = 7.067087342896948 \times 10^{10}\ N/m^2$ | $d_{31} = 3.777173702336798 \times 10^{-10}\ m/V$ |
| $c_{Db} = 2.367708630194484 \times 10^6\ Ns/m^2$ | $x_1 = 0.02041\ m$ |
| $\hat{x} = 0.11076\ m$ | $x_2 = 0.04592\ m$ |
| $\gamma = 7.659576963836054 \times 10^{-2}$ | |

Table 1: Measured and calculated beam and patch parameters

and $\hat{x}$ is the location of the proximity probe.

The hope is then to use this first order ODE to approximate the actual beam model, which approximates an actual beam if modelling assumptions hold up. However, this model is incomplete until parameters are specified. To this end, an inverse or parameter estimation problem is formulated. To solve the inverse problem we made use of a data set generated by a transient pulse sent to the front patch of the beam and scaled model observations. A Nelder-Mead algorithm was used to find a suitable fit with a cost functional that accounted for not only the time-space measures but also the frequency content of the beam. Table 1 lists all of the parameters, including those that were estimated in the inverse problem ($\rho_b$, $c_{Db}$, $E_b$, $\rho_p$, $c_{Dp}$, $E_p$, $d_{31}$, and $\gamma$) and those that were measured (all others). Figure 2 exhibits the scaled displacements of the data (in red) against the model (in blue). This figure is a good indication that the model is capable of taking on the characteristics (shape, frequency, etc.) of an actual beam vibration. From here on in we shall refer to the finite dimensional approximation of the Euler-Bernoulli beam model provided by equation (2.12) with the parameters given in Table 1 as the "virtual beam".

# 3 Proper Orthogonal Decomposition Based Model Reduction

In this section we outline the process used to reduce the size of the basis used for the Galerkin approximation, so as to allow for ease of real time implementation. The POD reduced order basis method is a transformation of a data set into an optimal set of POD modes that are orthonormal. In the case of the virtual beam, the data set (known as the *ensemble* of data) is a set of $N_s$ temporal snapshots, $\{y(t_j, x)\}_{j=1}^{N_s}$, of the virtual beam with a sinusoidal exogenous force over a certain time span. The POD method seeks functions $\Phi_i(x)$, $i = 1, 2, ..., N_p$, such

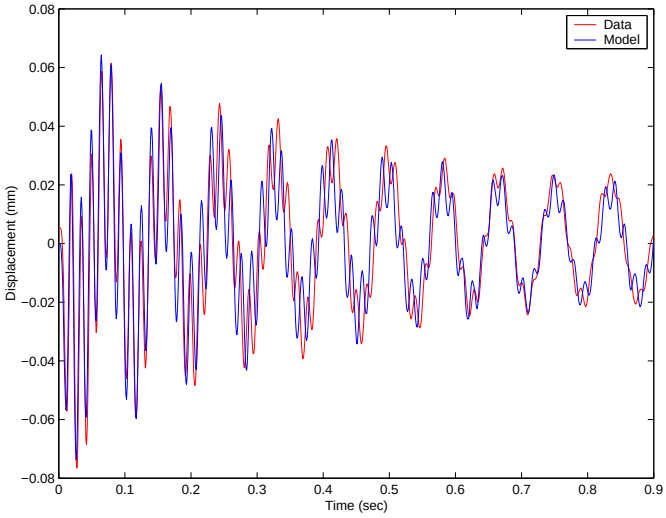


Figure 2: Measured and modeled beam displacement at proximity probe located at $\hat{x} = 0.11076m$

that each is a linear combination of the temporal snapshots given by

$$\Phi_i(x) = \sum_{j=1}^{N_s} \alpha_j^i y(t_j, x). \tag{3.13}$$

It is ensured that each of these basis elements resemble the data by requiring that the $i^{th}$ basis element maximizes

$$\frac{1}{N_s} \sum_{j=1}^{N_s} |\langle y(t_j, \cdot), \Phi_i(\cdot) \rangle| \ , \quad \text{subject to } \langle \Phi_i, \Phi_i \rangle = \|\Phi_i\|^2 = 1 \ ,$$

when the $\Phi_1, \ldots, \Phi_{i-1}$ are excluded. This condition also ensures that the POD elements are ordered such that the first basis element best characterizes the system, followed by the second, etc. To find the coefficients $\alpha_j^i$ in (3.13), the covariance matrix of the temporal snapshots, given by

$$[L]_{k,\ell} = \frac{1}{N_s} \langle y(t_k, \cdot), y(t_\ell, \cdot) \rangle \ , \quad k, \ell = 1, \ldots, N_s \ ,$$

is constructed. Then the eigenvalues (and corresponding eigenvectors) of $L$ are ordered from largest to smallest (this is possible because $L$ is nonnegative and Hermitian) so that $\lambda_1 \geq \lambda_2 \geq \cdots \geq \lambda_{N_s}$. It has been shown that the coefficient $\alpha_j^i$ corresponds to the $j^{th}$ entry of the $i^{th}$ eigenvector. To reduce the basis, we seek the smallest $N_p$ such that $\frac{\sum_{i=1}^{N_P} \lambda_i}{\sum_{i=1}^{N_s} \lambda_i} \simeq 1$. This ratio is the mean square error when the first $N_p$ members of the reduced basis representation are eliminated. Hence, the closer the ratio is to unity the closer the reduced

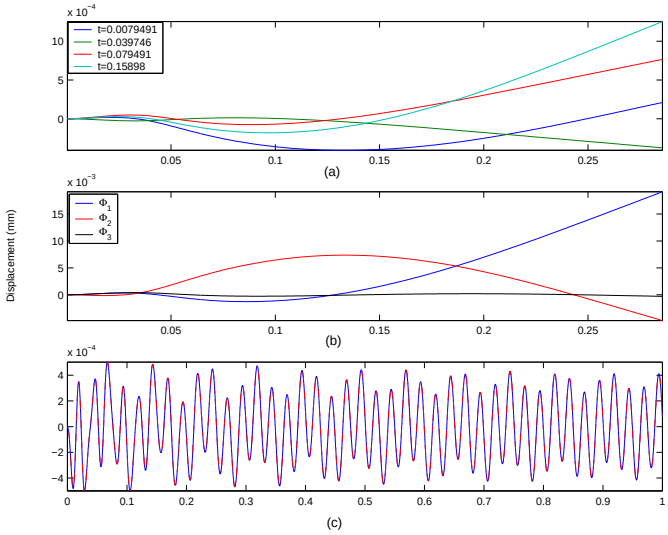


Figure 3: (a) Snapshots at times $10\delta t$ ($\delta t = 0.5/629$), $50\delta t$, $100\delta t$, and $200\delta t$ at 40 Hz, (b) First three POD modes, and (c) Comparison of uncontrolled dynamics using full order model (in blue) and POD reduced model (in red)

basis is to representing the entire Galerkin basis and thus the beam, given that sufficient system information was captured with the snapshots. Once $N_p$ is properly chosen , the basis elements are then used to construct system matrices by following the same methodology described in section 2.

We now present an example that illustrates the effectiveness of the POD model reduction. To produce the snapshots, we used the beam model with a sinusoidal disturbance of 40 Hz over the time span $0 \leq t \leq 0.5$. Through experimentation, we found that choosing the number of time snapshots such that $N_s = \lceil (2.5 \cdot \omega_d) \rceil$, $\omega_d$ being the radian frequency of the disturbance, is more than enough data for the reduction and is not too computationally taxing at the low frequencies of interest (20Hz through 50Hz) and besides, this is performed off-line, so the computational time is of little concern. Hence, for 40 Hz, we used 629 snapshots. Figure 3-(a) depicts four snapshots at $t = 10\delta t$ ($\delta t = 0.5/629$), $50\delta t$, $100\delta t$, and $200\delta t$ respectively. Through the POD method, we reduced the 17 element Galerkin basis down to three POD modes and obtained close to 100% accuracy in regenerating the snapshots (the captured energy associated with one, two, and three modes is reported in Table 2). The first three POD modes are represented graphically in Figure 3-(b). In Figure 3-(c), the uncontrolled virtual beam (in blue) and reduced model (in red) solutions are presented and are fairly indistinguishable.

| $N_P$ | 1 | 2 | 3 |
|---|---|---|---|
| $\sum_{i=1}^{N_P} \lambda_i / \sum_{i=1}^{N_s} \lambda_i$ | 0.7312353 | 0.9995505 | 0.9999989 |

Table 2: Energy contained in first three POD modes at 40 Hz

# 4 Control Methodology

## 4.1 LQR Compensation

In this section, we briefly describe techniques for formulating a state feedback control law and state estimations used in conjunction with these control laws to produce compensated systems . In the infinite horizon, consider the minimization of the quadratic cost functional

$$J(u, w_0) = \int_0^\infty (w^T Q w + u^T R u) dt$$

with associated linear state dynamics and output

$$\begin{aligned} &\dot{w}(t) = Aw(t) + Bu(t) \ , \quad w(0) = w_0 \ , \\ &w_{ob}(t) = Cw(t) \ . \end{aligned} \tag{4.14}$$

The weight matrices $Q > 0$ and $R \geq 0$ are design parameters. Making use of the calculus of variations it can be shown that the control that minimizes $J$ subject to the dynamics of $w$ is the state feedback control law described by

$$\begin{aligned} &u = -Kw \ , \\ &K = R^{-1} B^T \Pi \ , \end{aligned} \tag{4.15}$$

where $\Pi$ satisfies the so-called Riccati equation,

$$\Pi A + A^T \Pi - \Pi B R^{-1} B^T \Pi + Q = 0 \ .$$

For the virtual or CRSC beam, the states cannot all be measured and thus a state estimator or observer must be designed. Consider the estimation $w_e(t)$ governed by the dynamics and observations described by

$$\begin{aligned} &\dot{w}_e(t) = Aw_e(t) + Bu(t) + G(w_{ob}(t) - Cw_e(t)) \ , \\ &w_e(0) = w_{e_0} \quad \text{arbitrary} \ . \end{aligned} \tag{4.16}$$

Using the same techniques used to obtain the optimal control of equation (4.15) on the dual of system (4.14) one can obtain an optimal observer of the form (4.16) with gain $G$ described by

$$G = \hat{\Pi} C^T \hat{R}^{-1} \ ,$$

where $\hat{\Pi}$ satisfies the Riccati equation

$$\hat{\Pi} A^T + A \hat{\Pi} - \hat{\Pi} C^T \hat{R}^{-1} C \hat{\Pi} + \hat{Q} = 0 \ .$$

The matrices $\hat{Q}$ and $\hat{R}$ are design criteria for the state estimator that serve a similar role to that of $Q$ and $R$ in the optimal control problem. This observer converges to the state asymptotically so long as the system is detectable. This along with continuity then implies that the compensated controller,

$$\begin{aligned} u &= -Kw_e \ , \\ K &= R^{-1}B^T\Pi \ , \end{aligned}$$

will stabilize system (4.14).

## 4.2 Known Disturbance

It is recognized that the plant we are dealing with does not have the form of equation (4.14) due to the forcing term $Fg$ (see equation (2.12)). We seek to determine stabilization control of this forcing term. One way to attempt to accomplish this is to proceed with optimal control theory criterion as in the unforced case. Define a quadratic finite horizon cost functional to be

$$J(u, w_0) = \frac{1}{2}w(t_f)^T\Pi_f w(t_f) + \int_0^{t_f}(w^TQw + u^TRu)dt \ ,$$

where $\Pi_f \geq 0$, $Q > 0$, $R \geq 0$ are design parameters, as in the unforced case. Then by enforcing optimality conditions and making use of the sweep method one may determine the optimal controller to be described by the system

$$\begin{aligned} -\dot{\Pi} &= \Pi A + A^T\Pi - \Pi BR^{-1}B^T\Pi + Q \ , \quad \Pi(t_f) = \Pi_f \ , \\ K &= R^{-1}B^T\Pi \ , \\ -\dot{v} &= (A - BK)^Tv + \Pi Fg \ , \qquad\qquad\qquad v(t_f) = v_f \ , \\ u &= -Kw + R^{-1}B^Tv \ . \end{aligned}$$

Here, $(A, B, F)$ correspond to system matrices associated with either the Galerkin basis or the POD basis. Under certain conditions of stabilizability and detectability, as $\Pi$ and $v$ propagate backward in time and $t_f \to \infty$, $\Pi$ will reach a steady state, which we will denote by the same, and $v$ will converge to a periodic function with fundamental period equal to that of the sinusoidal disturbance. Thus, a suboptimal controller can be formulated in the following manner. Take $t_f$ sufficiently large to ensure the convergence mentioned above and solve for $v(t)$ backward in time, with $v(t_f) = 0$. Store a period of $v(t)$ forward in time and repeat it to produce $v_\infty(t)$, which is $v(t)$ on the infinite horizon. This results in the suboptimal affine controller described by

$$\begin{aligned} u &= -Kw + R^{-1}B^Tv_\infty \ , \\ K &= R^{-1}B^T\Pi \ . \end{aligned} \tag{4.17}$$

where $\Pi$ is the solution to the algebraic Riccati-equation

$$\Pi A + A^T\Pi - \Pi BR^{-1}B^T\Pi + Q = 0 \ .$$

As stated in subsection 4.1, we cannot measure the state and thus make use of observations in conjunction with a state estimator to develop a compensated system controller. In this setting the observer takes the form

$$\begin{aligned} &\dot{w}_e(t) = Aw_e(t) + Bu(t) + Fg(t) + G(w_{ob}(t) - Cw_e(t)) \ , \\ &w_e(0) = w_{e_0} \qquad \text{arbitrary} \ , \end{aligned} \tag{4.18}$$

where the optimal observer gain is provided by

$$\begin{aligned} &\hat{\Pi}A^T + A\hat{\Pi} - \hat{\Pi}C^T\hat{R}^{-1}C\hat{\Pi} + \hat{Q} = 0 \ , \\ &G = \hat{\Pi}C^T\hat{R}^{-1} \ . \end{aligned}$$

It is readily shown that, under sufficient conditions, the state estimator error converges asymptotically to the true state.

## 4.3 Frequency Shaped Feedback Control

Here we describe an alternative to the approach of subsection 4.2 as described in [12]. If the frequency behavior of the beam is known, a quadratic frequency domain cost functional,

$$J(u) = \frac{1}{2}\int_0^\infty \left(w^*(i\omega)Q(i\omega)w(i\omega) + u^*(i\omega)Ru(i\omega)\right) d\omega,$$

developed using realization theory, can be used to penalize these frequencies in addition to the states. In our case, we resolved to inhibit the lowest resonant frequency of the beam, $\omega_r$, and the disturbance frequency, $\omega_d$. In [8], it was explained that minimizing $J$ corresponding to these two frequencies is equivalent to minimizing the cost functional associated with the augmented system $\dot{z} = \tilde{A}z + \tilde{B}u + \tilde{F}g$, written explicitly as

$$\begin{bmatrix} \dot{w} \\ z_1^r \\ z_2^r \\ z_1^d \\ z_2^d \end{bmatrix} = \begin{bmatrix} A & 0 & 0 & 0 & 0 \\ 0 & 0 & 1 & 0 & 0 \\ B_r & -\omega_r^2 & -2\omega_r\xi_r & 0 & 0 \\ 0 & 0 & 0 & 0 & 1 \\ B_d & 0 & 0 & -\omega_d^2 & -2\omega_d\xi_d \end{bmatrix} \begin{bmatrix} w \\ z_1^r \\ z_2^r \\ z_1^d \\ z_2^d \end{bmatrix} + \begin{bmatrix} B \\ 0 \\ 0 \\ 0 \\ 0 \end{bmatrix} + \begin{bmatrix} F \\ 0 \\ 0 \\ 0 \\ 0 \end{bmatrix} g(t) \ . \tag{4.19}$$

Here, $(A, B, F)$ are either the Galerkin basis system matrices or the POD basis system matrices, $w$ is the state vector, $\xi_r$ and $\xi_d$ are shaping parameters that determine the frequency band of the filter implicitly implemented, and $B_r$ and $B_d$ are $1 \times n$ vectors with $\omega_r^2$ and $\omega_d^2$ as values (respectively). This system is coupled with the observation equation

$$z_{ob}(t) = \begin{bmatrix} C & 0 & 0 & 0 & 0 \end{bmatrix} z = \tilde{C}z \ .$$

Since the system state requires estimation, as in subsection 4.2, we use the techniques described in subsection 4.1 to formulate the observer

$$\begin{aligned} &\dot{z}_e(t) = \tilde{A}z_e(t) + \tilde{B}u(t) + \tilde{F}g(t) + G(z_{ob}(t) - \tilde{C}z_e(t)), \\ &z_e(0) = z_{e_0} \quad \text{arbitrary} \ . \end{aligned} \tag{4.20}$$

The states appended to the beam system correspond to a minimal realization of a filter in the frequency space. Thus, these states are controllable and observable and hence, so long as $(A, B)$ and $(A^T, C^T)$ have the desired controllability, the methods of subsection 4.1, applied to unforced linear system $(\tilde{A}, \tilde{B}, \tilde{C})$, can be used to determine a control for the beam.

# 5 Implementation in Simulation

In this section we discuss some aspects of the real time implementation of the proposed control methodologies, provide a sample of simulation results, and discuss these results. The primary implementation issue, from a mathematical control perspective, is the fact that the beam model is continuous and the controls developed based on this model are likewise continuous. However, the tools used to extract measurements and to produce inputs for the system are discrete in nature, being capable of action only at a particular frequency, say $\Delta t^{-1}$ samples per second, that is limited by processor speed, etc. Thus, it is necessary to determine how to circumvent this issue and still make use of the model and controls developed. The way to do this is to take advantage of continuity and the fact that the actual sampling frequency of instrumentation is high.

As discussed, feedback of the beam state is not directly possible because the state is not all measurable. Thus an observer is used. This observer is described by equation (4.18) in one case and (4.20) in another. Both depend on instantaneous knowledge of the actual observation, which is only obtainable every $\Delta t$ seconds, and both require the use of an ODE solver. Thus, it is typical to march the observer forward in time using the backward Euler method in correspondence with the observation frequency. It is noted that other integration methods and methods of dealing with the discrete nature of the observations, such as interpolation, could be used. However, the backward Euler method is simple, unconditionally stable, and computationally efficient (especially in a reduced order setting), as most of the calculation involved occurs off-line. The approximation of $w_e^{n+1}$ is then

$$
\begin{aligned}
&w_e^{n+1} = R_{\Delta t}^{-1}(w_e) w_e^n + \Delta t R_{\Delta t}^{-1}(w_e) F g_{n+1} + \Delta t R_{\Delta t}^{-1}(w_e) G {w_{ob}}^{n+1} \ , \\
&R_{\Delta t}^{-1}(w_e) = \begin{cases} (I - (A - BK - GC))^{-1} & \text{controlled} \ , \\ (I - (A - GC))^{-1} & \text{uncontrolled} \ , \end{cases} \\
&w_e^0 = 0 \ .
\end{aligned}
$$

Here $(A, B, C, F)$ are system matrices that may correspond to the Galerkin basis, the POD basis, or either of these systems with frequency shaping states added; $G$ and $K$ are, respectively, the observer gain and feedback control gain corresponding to this system; and $g_{n+1} = g((n+1)\Delta t)$. From this scheme one can predict, given ${w_{ob}}^{n+1}$, $g_{n+1}$, and $w_e^n$, $w_e^{n+1}$. A similar scheme, with an additional term due to the affine form of the controller, is used for (4.18). Since $g$ is known and $w_e^0$ is chosen, the only issue is the value of ${w_{ob}}^{n+1}$, which is not known. Calling on continuity it can be claimed that for small $\Delta t$, ${w_{ob}}^{n+1} \approx {w_{ob}}^n$. Making

this approximation provides

$$w_e^{n+1} = R_{\Delta t}^{-1}(w_e)w_e^n + \Delta t R_{\Delta t}^{-1}(w_e)Fg_{n+1} + \Delta t R_{\Delta t}^{-1}(w_e)G{w_{ob}}^n \tag{5.21}$$

as a modified backward Euler scheme. With this prediction of $w_e^{n+1}$ the compensation control at the next time step is predicted and taken to be $u_{n+1} = -Kw_e^{n+1}$.

We have implemented this scheme with the control techniques of section 4 in numerical simulation. This was accomplished by using the virtual beam. We sampled observations from this beam and levied the controls on it just as we would the CRSC beam. The virtual beam dynamics and observations were simultaneously marched forward with the observer and control. The $(n+1)^{st}$ iterate of the virtual beam dynamics is

$$\begin{aligned}
w^{n+1} &= \begin{cases} R_{\Delta t}^{-1}(w)w^n + \Delta t R_{\Delta t}^{-1}(w)Fg_{n+1} & \text{uncontrolled ,} \\ R_{\Delta t}^{-1}(w)w^n + \Delta t R_{\Delta t}^{-1}(w)Bu_{n+1} + \Delta t R_{\Delta t}^{-1}(w)Fg_{n+1} & \text{controlled ,} \end{cases} \\
w_{ob}^n &= Cw^n \ , R_{\Delta t}^{-1}(w) = (I - \Delta t A)^{-1} \ , \\
w^0 &= w_0 \ .
\end{aligned}$$

Here $(A, B, C, F)$ are the virtual beam system matrices and $u_n$ is the control iterate constructed from the observer and the particular controller.

# 6 Discussion of Simulation

For simulation, we selected the external disturbance by taking $g = F_{mag}\sin(\omega_d t)$, where $F_{mag}$ is a conglomeration of several factors that relate to experimental equipment, etc., used in the setup of the CRSC beam. In this way we stayed consistent with the beam we will use for actual implementation. $\omega_d$ was selected to place the source in the low narrowband of 20 to 60 Hz.

In regards to the selection of an actual controller to implement in simulation there is much to be considered. To select a controller instance is to select the design parameters $(Q, R, \hat{Q}, \hat{R})$ in accordance with what is to be accomplished. For implementation, both in simulation and experimental setting, we have made use of the Matlab (The MathWorks Inc.) routine `lqr` to obtain a numerical solution to the Riccati equations associated with the design parameters. Thus obtaining $\Pi$ and $\hat{\Pi}$ for the construction of controls and observers. This in itself presents problems. Firstly, for some theoretically legitimate designs, the `lqr` routine fails, returning an error message related to numerical problems instead of $\Pi$ or $\hat{\Pi}$. Therefore we have been limited in design to those parameters accepted by `lqr`. This is a problem, as open exploration is prohibited. Secondly, in many cases, solutions that the `lqr` routine will produce are not accurate. That is, for some design parameters the values of $\Pi$ and $\hat{\Pi}$ returned by `lqr` do not come close to solving the Riccati equations. Thus we have been further restricted to keeping only those designs where the `lqr` results actually satisfy, at an acceptable level, the Riccati equations. This is a restriction not made in some previous

| Model | Frequency Shaping | Affine |
|---|---|---|
| Full State | $\mu = 5 \times 10^{0}$ , $\sigma = 1 \times 10^{-2}$ , $\hat{\mu} = 1 \times 10^{-1}$ , $\hat{\sigma} = 1 \times 10^{0}$ . | $\mu = 5 \times 10^{8}$ , $\sigma = 1 \times 10^{-1}$ , $\hat{\mu} = 1 \times 10^{7}$ , $\hat{\sigma} = 1 \times 10^{-1}$ . |
| POD | $\mu = 5 \times 10^{11}$ , $\sigma = 1 \times 10^{4}$ , $\hat{\mu} = 1 \times 10^{0}$ , $\hat{\sigma} = 1 \times 10^{-1}$ . | $\mu = 5 \times 10^{11}$ , $\sigma = 1 \times 10^{3}$ , $\hat{\mu} = 1 \times 10^{10}$ , $\hat{\sigma} = 1 \times 10^{-1}$ . |

Table 3: Scalars defining the control design parameters of 6.22 used in simulation.

experimental studies and thus some earlier presented results in the implementation direction are not accurate in the sense that the controllers ultimately employed were not truly based on LQR theory because the controls and observers are not associated with true solutions to the Riccati equations. Again, we have had to give up many of the designs we would have liked to obtain results for. Lastly, many of the designs that avoid the problems above produce controls and observers that simply do not comply with our objectives. It has been said that selection of LQR design parameters is more an art than a science. We have found it to be neither, as there is nothing aesthetically pleasing about guessing parameters.

In order to avoid guessing we took cues from the work of the authors of [23] and [12]. For controller design we select

$$\begin{aligned} Q &= \mu \begin{bmatrix} K & 0 \\ 0 & M \end{bmatrix} \quad , \quad R = \sigma \ , \\ \hat{Q} &= \hat{\mu} \begin{bmatrix} I^{N+1} & 0 \\ 0 & I^{N+1} \end{bmatrix} \quad , \quad \hat{R} = \hat{\sigma} \ . \end{aligned} \tag{6.22}$$

For results presented herein $(\mu, \sigma, \hat{\mu}, \hat{\sigma})$ takes on the values provided in table 3, which are for the most part in accordance with [23] and [12]. Surely we make no claims that this selection is optimal, but it works.

In Figure 4 simulation results for 40 Hz are presented as a sample of our better findings. More could be shown but all are similar and there is little to be demonstrated by doing so. This one figure is enough to illustrate comments that generalize to all such results we obtained. In these simulations the beam was driven uncontrolled for approximately 3 periods corresponding to the resonant frequency $\omega_r$ and then the controller was turned on. Let it be emphasized that these figures represent the response of the virtual beam to model based controllers implemented in a real time fashion through use of state estimates based on actual observations. In this light, certain features of these results are quite promising. First note that $(a)$ and $(b)$ indicate that both control designs can work, both in the Galerkin and in the POD reduced order regimes. This is rather impressive in the following sense. If the virtual beam used actually mimics beam like activity, then the POD results indicate that one could actually forego dependence on the parameter dependant PDE model of (2.1). That is, it would seem that, given sufficient equipment, we could take snapshots of the actual beam, construct the POD model from actual data, and formulate controllers using this model.

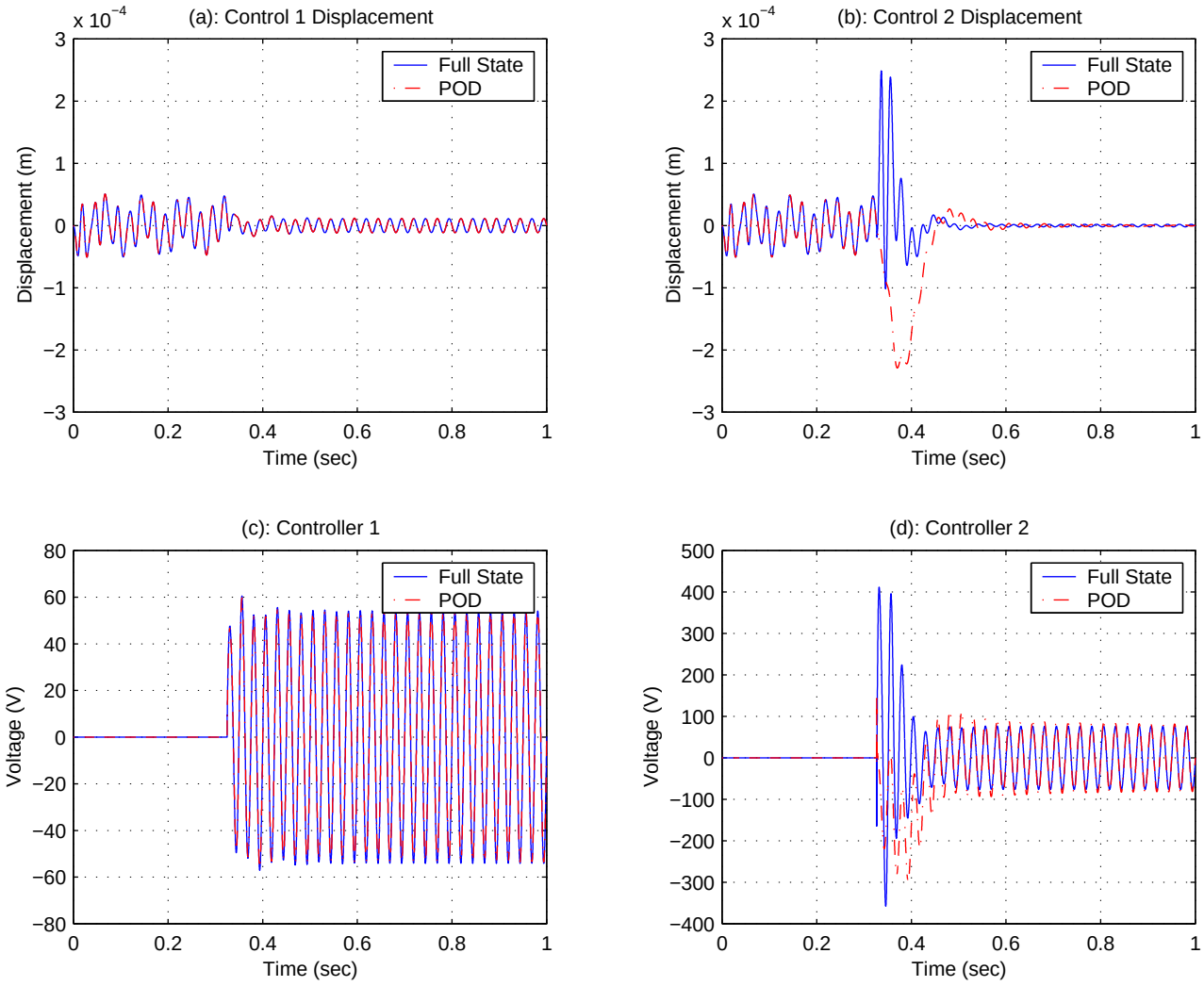


Figure 4: $(a)$: Displacements controlled by the affine controller (4.17), $(b)$: Displacements controlled by frequency shaping, $(c)$: The affine controller (4.17), and $(d)$: The frequency shaping controller.

The second thing we note is that $(b)$ verifies the nice results of [12] and extends them to functionality.

Also, comparing $(a)$ to $(b)$ and $(c)$ to $(d)$, some of the advantages and disadvantages of both relative to one another are seen. The frequency shaping filtering seems to have the greater potential to really attenuate the effects of a periodic source. However the method is perhaps too aggressive. Looking at the control voltages used to produce these results it is seen that when the frequency shaping controller is turned on it drives the beam too hard, causing some accentuated displacements in the structure that may be destructive. Beyond that ill-effect is the problem that the control voltages initially demanded by the frequency shaping method are not really feasible. For instance, for the CRSC laboratory setup, the voltage limits are $\pm 100V$. We did find that careful selection of the time at which the controller is turned on can lessen this effect, but the problem is persistent. It is seen that after a tenth of a second or so the control is within a suitable range, but we also discovered that that tenth of a second makes all the difference. In a vain attempt to avert the problem we composed the controller with a saturation function with suitable range. The controller then failed. Of course, increasing the design parameter $R$ was also attempted. This does reduce the control effort but the pole placement that made the method so promising is lost. On the other hand, the affine controller makes the transition from uncontrolled to controlled in a smooth fashion, causing no displacements beyond those caused by the disturbance and maintaining a control magnitude that is very reasonable in the sense that we could produce this control in the CRSC laboratory. From a practical point of view these observations may suggest that one could use the affine controller to subdue the beam and then employ the frequency shaping method to further attenuate the disturbance. It might also be of interest to attempt sequential update of the control gain corresponding to a sequential alteration of design parameters, so as to ease the beam into the desired behavior over time.

# 7 Conclusion

In this paper we have provided the essential details of a feasibility study currently underway that focuses on the real time implementation of feedback controllers designed to reduce vibrations in a cantilevered beam with surface mounted piezoelectric actuators. The impetus for such an undertaking is multifaceted. Firstly, the study of the cantilevered beam in the smart-structure setting serves as a starting point for the general development of control methodologies for smart structures of this type. Namely, thin shells and plates with surface mounted or embedded PZTs. Secondly, the inclusion of frequency information in the determination of optimal controls developed in the setting of modern control theory is a topic of interest. The frequency shaping method is a technique that realizes such a goal. Clearly this is of great interest in applications such as model based vibrational control in structures. Thus, the vibration control of the cantilevered beam provides an excellent context for testing the applicability of this control methodology. Thirdly, for all proposed model based control,

there is an interest in the utility of the POD model reduction process. This is due to the fact that the method is still under scrutiny having arguments both in favor and against its use. The use of this method in this particular context has shown great promise thus far and here we have sought to further support its potential by successfully employing the method in conjunction with different control approaches. Finally, of most interest is whether all of these ideas can or cannot come together in an actual real time implementation. As expected, what we have discovered so far shows some promise and revealed some issues that need further investigation.

In nearly every real time simulation we have ran, POD, with good sampling, has provided an excellent model. We mean this in the sense that this model provides displacements comparable to those provided by a Galerkin based approximation to the solution of the dynamics of the structure and the controls based on the POD model appear to work just as well as those based on the Galerkin type approximations. Also promising is the use of frequency shaping control methods in this setting. In fact, the frequency shaping method described herein seemed to have a greater potential for the attenuation of a periodic exogenous force than control simply based on optimality criterion for minimization of typical cost functionals involving state-space measures.

On the other hand, there is simply a lot of work yet to be done. The most prominent of tasks to be addressed is as follows:

1. Determine parameters that realize a model that mimics the behavior of the actual beam we intend to use in actual experimentation.

2. Consider procedures that may help with controller design and in easing the numerical difficulties in determining optimal gains via Riccati equation solutions.

3. Investigate methods of introducing frequency shaping controllers within equipment limitations and without invoking violent displacements of the beam.

In future work we will address the above issues and also will consider other control approaches, including the so-called filtered-x and hybrid controls discussed in [12]. Additionally, we hope to not only apply these ideas through numerical simulation, but also in actual experimentation in the CRSC laboratory.

**Acknowledgement**: We would like to thank Dr. Hien T. Tran for offering continued support and insight throughout the experimentation and implementation. Also, James M. Nealis and Jordan E. Massad for their input at the inception of the project.

# References

[1] J.A. Atwell and B. King, *Proper Orthogonal Decomposition for Reduced Basis Feedback Controllers for Parabolic Equations*, ICAM Rep. 99-01-01, VPISU, Blacksburg, VA, January, 1999; Mathematical and Computer Modeling, to appear.

[2] J.A. Atwell and B. King, *Reduced Order Controllers for Spacially Distributed Systems via Proper Orthogonal Decomposition*, ICAM Rep. 99-07-01, VPISU, Blacksburg, VA, July, 1999.

[3] N. Aubry, P. Holmes, J. Lumley, and E. Stone, *The Dynamics of Coherent Structures in the Wall Region of a Turbulent Boundary Layer*, Jounal of Fluid Mechanics, 192 (1988), pp. 115-173.

[4] H.T. Banks, K. Ito, and Y. Wang, Well Posedness for Damped Second Order Systems with Unbounded Input Operators, CRSC Technical Report CRSC-TR93-10, June, 1993; *Differential and Integral Equations*, 8(3), 1995, pp. 587-606.

[5] H.T. Banks, R.C. Smith, and Y. Wang, *Smart Material Structures: Modeling, Estimation, and Control*, Masson/John Wiley, Paris/Chichister, 1996.

[6] G. Berkooz, P. Holmes, and J. Lumley, *The Proper Orthogonal Decomposition in the Analysis of Turbulent Flows*, Annual Review of Fluid Mechanics, 25 (1993), pp. 539-575.

[7] G. Berkooz, P. Holmes, J. Lumley, and J.C. Mattingly, *Low Dimensional Models of Coherent Structures in Turbulence*, Physics Report-Review Section of Physical Letters, 287 (1997), pp. N4:338-384.

[8] N.K. Gupta, Frequency-Shaped Cost Functionals: Extension of Linear-Quadratic-Guassian Design Methods, *Journal of Guidance and Control*, 3(6), 1980.

[9] A. Iollo, S. Lanteri, and J.A. Desideri, *Stability Properties of POD-Galerkin Approximations for the Compressible Navier Stokes Equations*, INRIA Rep. de Rech. no. 3589, December, 1998; Sophia Antipolis.

[10] G.M. Kepler, H.T. Tran, and H.T. Banks, *Compensator Control for Chemical Vapor Deposition Film Growth Using Reduced Order Design Models*, CRSC-TR99-41, North Carolina State University, Raleigh, NC, December, 1999; IEEE Trans. Semi-conductor Manuf., submitted.

[11] G.M. Kepler, H.T. Tran, and H.T. Banks, *Reduced Order Comensator Control of a Species Transport in a CVD Reactor*, tech rep., CRSC-TR99-15, North Carolina State University, Raleigh, NC, April, 1999; Optimal Control: Applications and Methods, submitted.

[12] D.J. Kolepp and R.C. Smith, Narrowband Control Design for Smart Structural Systems, CRSC Tecnical Report CRSC-TR01-30, November, 2001.

[13] K. Kunisch and S. Volkwein, *Control of Burger's Equation by Reduced Order Approach Using Proper Orthogonal Decomposition*, Optimierung und Kontrolle Bericht no. 138, Universitat Graz, Austria, September, 1998; J. Opt. Theory Applic., to appear.

[14] J. Lumley, *The Structure of Inhomogeneous Turbulent Flows*, Atmospheric Turbulence and Wave Propagation, (1967), pp. 166-178.

[15] H. Ly and H. Tran, *Modeling and Control of Physical Processes Using Proper Orthogonal Decomposition*, tech. rep., CRSC-TR98-37, North Carolina State University, Raleigh, NC, November, 1998; Journal of Computational and Computer Modeling, to appear.

[16] H. Ly and H. Tran, *Proper Orthogonal Decomposition for Flow Calculations and Optimal Control in a Horizontal CVD Reactor*, tech. rep., CRSC-TR98-13, North Carolina State University, Raleigh, NC, November, 1998; Quarterly of Appled Mathematics, to appear.

[17] D. Nagy, *Model Representation of Geometrically Nonlinear Behavior by the Finite Element Method*, Computers and Structures, 10(1979), pp. 683-688.

[18] A. Noor, *Recent Advances in Reduction Methods for Nonlinear Problems*, Computers and Structures, 10 (1981), pp 31-44.

[19] A. Noor, C. Anderson, and J. Peters *Reduced Basis Technique for Collapse Analysis of Shells*, AIAA Jounal, 19 (1981), pp 393-397.

[20] A. Noor and J. Peters *Reduced Basis Technique for Nonlinear Analysis of Structures*, AIAA Jounal, 18 (1980), pp 455-462.

[21] J. Peterson, *The Reduced Basis Method for Incompressible Viscous Flow Calculations*, SIAM Journal on Scientific and Statistical Computing, 10 (1989), pp. 777-786.

[22] L. Sirovich, *Chaotic Dynamics of Coherent Structures*, Physica D, 37 (1989), pp. 126-145.

[23] R.C.H. del Rosario, H.T. Tran, and H.T. Banks, Proper Orthogonal Decomposition Based Control of Transverse Beam Vibrations: Experimental Implementation, CRSC Technical Report CRSC-TR99-43, December, 1999.

[24] A. Theodoropolou, R.A. Adomaitis, and E. Zafiriou, *Model Reduction for Optimization of Rapid Thermal Chemical Vapor Deposition Systems*, IEEE Trans. Semiconductor Manuf., 11 (1998), pp. 85-98.